Design and Kinetostatic Modeling of a Cable-Driven Schönflies-Motion Generator

Giuseppe Sciarra, Tahir Rasheed, Valentina Mattioni, Philippe Cardou, Stéphane Caro

Proceedings of the ASME 2022 International Design Engineering Technical Conferences & Computers and Information in Engineering Conference
IDETC/CIE 2022
August 14-17, 2022, St. Louis, Missouri, USA

IDETC2022-89384

DESIGN AND KINETOSTATIC MODELING OF A CABLE-DRIVEN SCHÖNFLIES-MOTION GENERATOR

Giuseppe Sciarra[1,2], **Tahir Rasheed**[1,3], **Valentina Mattioni**[2], **Philippe Cardou**[4], **Stephane Caro**[1,3]
[1] Nantes Universite, Laboratoire des Sciences du Numerique de Nantes (LS2N), UMR CNRS 6004, 44300 Nantes, France
[2] Department of Industrial Engineering, University of Bologna, 40137 Bologna, Italy
[3] Centre National de la Recherche Scientifique (CNRS), 44321 Nantes, France
[4] Laboratoire de robotique, Département de génie mécanique, Université Laval, Québec, QC, Canada
Emails: giuseppe.sciarra@studio.unibo.it, tahir.rasheed@ls2n.fr, valentina.mattioni@unibo.it, pcardou@gmc.ulaval.ca, stephane.caro@ls2n.fr

ABSTRACT

Cable-Driven Parallel Robots (CDPRs) use cables to move a moving-platform in space offering different advantages, such as high payload, reconfigurability, large translational workspace and high dynamic performances. However, their orientational workspace is usually limited due to cable/cable and cable/moving-platform collisions. In this paper, a novel Schönfiles-Motion Generator (SMG) with a large translational workspace and a full rotation of its end-effector about a vertical axis is introduced. The full rotation of the end-effector is obtained using a parallelogram cable loop. It should be noted that the four degrees of freedom motion of the end-effector is controlled by four actuators fixed to the ground thanks to three parallelogram cable loops and a transmission system containing a differential mechanism. The kinetostatic model of the CDPR under design is expressed. The static workspace of the proposed Cable-Driven SMG (CDSMG) with three different cable arrangements is analyzed. Finally, a prototype of the CDSMG is presented and preliminary experimental results are discussed.

1 INTRODUCTION

Cable-Driven Parallel Robots (CDPRs) are a type of parallel manipulators, where rigid links are replaced by flexible cables that actuate the moving-platform (MP). Each cable has one side connected to the MP and the other end wound on a winch actuated by a motor rigidly fixed to the base. Passive pulleys are usually used to guide the cable from the winch to the MP. The pose of the MP is controlled by changing the cable lengths. CDPRs have advantages in terms of large translation workspace compared to classical parallel robots [1], heavy payload capacity [2], reconfigurability [3], and performing high-speed tasks [4].

A case when the reconfiguration is useful is when dealing with a cluttered environment, it is easy for the robot to collide with external objects, thus, moving the exit point will avoid the collision [5]. At the same time, by changing the robot setup, its workspace may be enlarged, as well, the stiffness and the payload capability. Cases where the reconfiguraility of a robot is well performed are: [6] and [7]. The reconfigurability of the robot makes things easier when a new prototype needs to be adapted to a pre-existent CDPR, it can be done, for example, by changing the platform, the exit point position and readapting the control scheme.

Despite their large translation workspaces, CDPRs are generally unable to provide large amplitudes of rotation of the MP due to collisions between their moving parts, such as cable/cable and cable/MP. The workspace of CDPRs can be increased by combining them with other parallel or serial mechanisms, constructing a hybrid system [8], [9]. For example, a parallel spherical wrist was used for the design of a CDPR to obtain both a large orientation workspace and a large trans-

lational workspace. Another example of hybrid mechanism dates back to 1999, Siciliano in [10] presented a robot in which a three-DOF spherical wrist is mounted on the moving platform of a three-DOF parallel manipulator.

The robot proposed in this paper features four motors and four degrees of freedom, namely, three translational motions and one rotational motion around a vertical axis. The full circle rotational motion of the end-effector is obtained by coupling a cable-loop and a pulley on the MP. The peculiarity of this robot is the arrangements of the cables around the MP. Indeed, the six cables of the proposed Cable-Driven Schönflies Motion Generator (CDSMG) are arranged in such a way that three parallelograms cable structures are formed to constrain the rotational motions of the MP [11–15]. One of the six cables is wound on two drums at its two ends, making one cable loop used to actuate the rotational motion of the pulley embedded in the MP. A novel transmission system containing a differential mechanism is synthesized to control with two actuators, mounted on the ground, the lengths of the two cables and the circulation of the cable-loop so that the parallelogram cable-loop is kept and the full circle rotational motion of the embedded pulley, namely, the end-effector, is ensured. Therefore, the CDSMG introduced in this paper is of a special class of motions named, for the serial robot, SCARA (selective-compliance assembly robot arm). It thus generates the same types of movements as those generated by the McGill SMG [16], but with greater amplitudes in translation and rotation. This paper aims to prove the effectiveness of the parallelogram cable-loop with a circulating cable in a three-dimensional space. A drawback related to the cable loop is the following: when the cable loop actuates the embedded pulley, the torque transmitted provides the tilts of the moving platform. This issue is solved by arranging the cables around the platform with parallelograms shapes. This drawback is due to the fully-constrained nature of this CDPR, which must exploit gravity to maintain its posture. This issue is less important in the case of overconstrained designs [17], [18]. A planar case of a CDPR without parasitic tilts is described in [19], where the authors demonstrated the efficacy of a robot architecture composed of a transmission system, a cable loop and a parallelogram.

The paper is organized as follows: the robot architecture is presented in Sec. 2. The overall kinetostatic model is expressed in Sec. 3. The static workspace of three arrangements of the CDSMG under study is analyzed in Sec. 4. Section 5 shows the prototype and preliminary experimental results in terms of parasitic MP tilt. Conclusions and future work are drawn in Sec. 7.

2 ROBOT ARCHITECTURE

Figure 1 presents the proposed robot architecture. Its architecture consists of a rectangular MP with an embedded

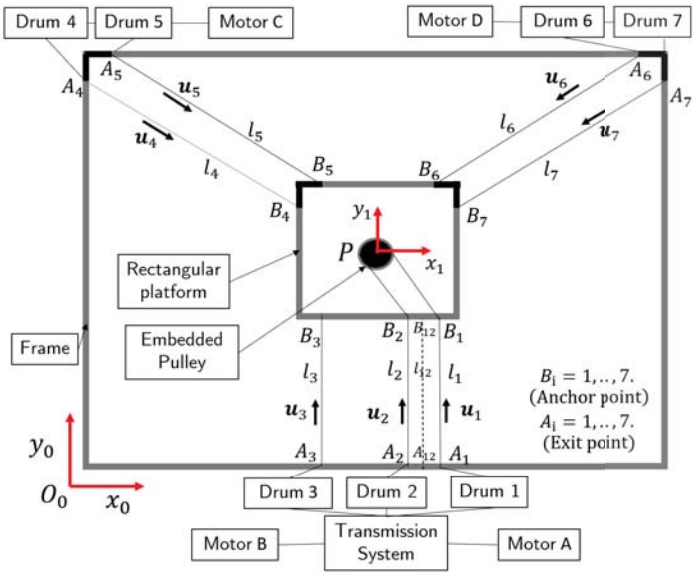

FIGURE 1: Top view of the CDSMG scheme

mechanism actuated by a cable-loop. The total number of cables is six, as the cable-loop is formed by a single cable, which can be represented with a virtual cable 12 (Fig. 1). The parallelogram architectures $A_{12}B_{12}B_3A_3$, $A_4B_4B_5A_5$ and $A_6B_6B_7A_7$ constrain the rotational motions of the MP. For simplicity of modelling, the cable-loop is split into two branches, respectively, cables 1 and 2. Attached to the ceiling of the frame, the exit points A_i guide the cables to the anchor points B_i. The distances between the exit point A_i and the anchor point B_i is the cable length l_i , i = 1,...,7. The unit vectors $\mathbf{u}_i$, i = 1,...,7, are the directions of the corresponding cables. $\mathscr{F}_0(O_0, x_0, y_0, z_0)$ is the fixed frame and $\mathscr{F}_1(P, x_1, y_1, z_1)$ is the frame attached to the MP.

The total number of drums is equal to seven. Three of them, namely, drum 1, 2 and 3, are actuated by two motors, namely, motor A and B, via a transmission module (see Sec. 2.2). The remaining four are driven by two motors: drums 4 and 5 (drums 6 and 7, resp.) are connected to motor C (motor D, resp.) through a common shaft in order to make sure the single cables of the corresponding parallelogram architectures keep the same length, as shown in Fig. 1.

The transmission module is located in the centre of the lower frame side. The exit points A_1, A_2, A_3 are located in the frame so that the cable remains vertical. While the exit points A_4, A_5, A_6, A_7 are located in such a way that the cables are farther as possible from each other, in that way the constraint moment generated by the parallelogram structure is bigger and the tilts are well prevented. On the contrary, if $B_4 = B_5$ and $A_4 = A_5$, the parallelogram won't provide any constraint moment.

2.1 Cable-Loop Principle

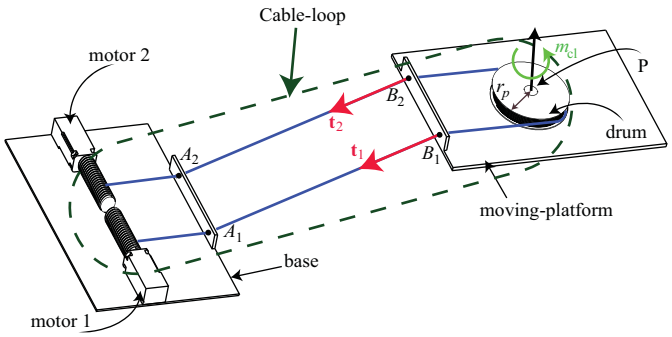

FIGURE 2: Cable-loop principle

The cable-loop (Fig. 2) has both of its ends coiled on separate winches, which in turn, are actuated by two motors as described in [9] and [20]. Eyelets are used to maintain constant exit-points, namely, A_1, A_2, and anchor-points, namely, B_1, B_2. The cable-loop is coiled around a pulley on the MP. This pulley then acquires one rotational degree-of-freedom (DOF) with respect to the MP, which is used either to actuate a tool or to control additional degrees of freedom such as rotations over wide ranges. The cable-loop has two purposes. First, translate the MP when the coiling speeds of both motors have the same magnitude and direction. Second, let the embedded pulley rotate by circulating the cable. It happens when both the motors have the same coiling speeds but in opposite directions.

2.2 Transmission System

The transmission system shown in Fig. 3, which is the core part of the robot, differs from the one used in [19]. It allows actuating three drums with only two motors. During the translational motion, the parallelogram shape made by cable 3 and the virtual cable 12 must be maintained. A differential mechanism ensures that the coiling speed of cable 3 is the mean of those of cables 1 and 2. This concept is explained in the flow chart depicted in Fig. 4. Belts and pulleys, with proper tensioners, are used to connect the motors with the differential. Motor A and motor B are directly connected to drum 3 and drum 1, respectively, through two shafts. A pulley-belt system permits the carrier to have the same velocity of motor A, the same system is adopted between motor B and one sun. Thus, the remaining sun is connected to drum 3.

The transmission module actuates the cable-loop as well. Being drum 1 and drum 2 connected to the differential suns gears, just actuating the motor B let the two drums rotate in the opposite direction with the same velocity, thus, the platform remains stationary while the embedded pulley is rotating. It is

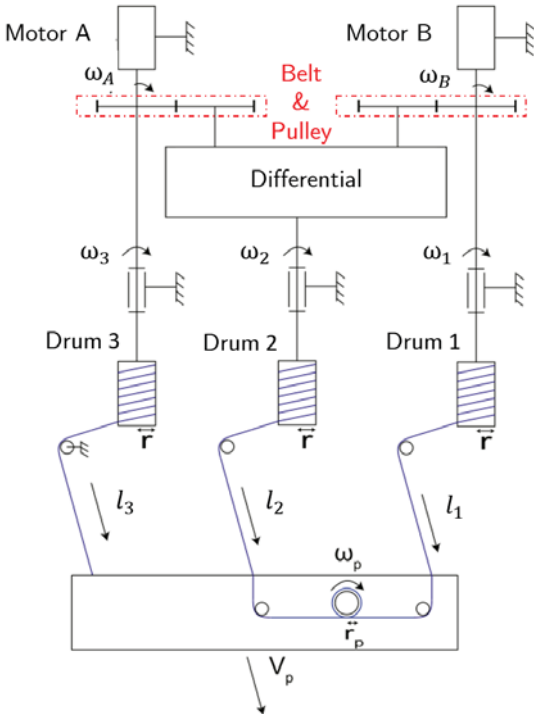

FIGURE 3: Transmission system scheme

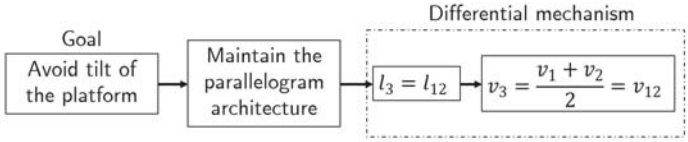

FIGURE 4: Relationships obtained through the differential mechanism

possible to actuate the cable-loop and at the same time move the platform; it happens when the velocity of cable 1 and cable 2, branches of the same cable-loop, are different. The difference in velocity of the two cables permits the pulley to rotate and the platform to move simultaneously. The following relationships give the angular velocity of the embedded pulley ω_p and the velocity of the virtual cable v_{12} as a function of v_1,v_2 and the radius of the embedded pulley, r_p:

$$\omega_p = \frac{v_1 - v_2}{2r_p} \tag{1}$$

$$v_{12} = \frac{v_1 + v_2}{2} \tag{2}$$

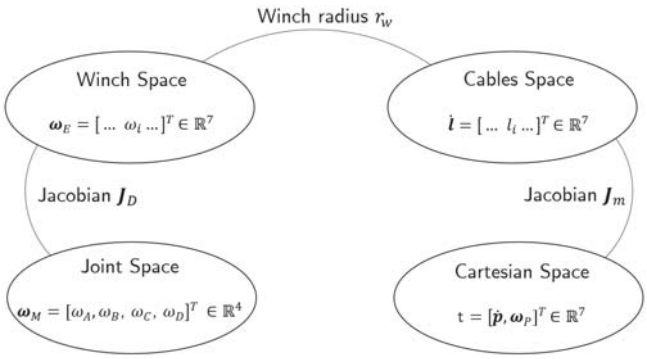

FIGURE 5: Joint, wrench, cable and Cartesian velocity spaces of the robot

2.3 Parametrization

The robot modelling includes four spaces: Cartesian space, cable-length space, winch space and joint space, as shown in Fig. 5. θ_A,θ_B,θ_C and θ_D are the motor position angles, l_i, $i = 1,\ldots,7$ are the cables lengths. x, y and z are Cartesian coordinates of the geometric center P of the MP. α is the cable loop pulley position angle, and roll, pitch, yaw are the azimuth, tilt and torsion angles of the MP. It should be noted that the parallelogram cable-loop shown in Fig. 3 guarantees the last three angles to be null under the assumption that the cables are inextensible and always in tension.

3 KINETOSTATIC MODELLING

This section aims to express the kinetostatic model, namely, the kinematic Jacobian matrices and the wrench matrix, of the CDSMG under study. First, the kinematic model of the transmission system is described. Then, the forward and inverse Jacobian matrices of the CDSMG are obtained while considering the kinematic Jacobian matrix of the transmission system.

3.1 Transmission modelling

The transmission guarantees to have the angular velocity of drum 3 equal to the average value of the angular velocity of drums 1 and 2:

$$\omega_3 = \frac{\omega_1 + \omega_2}{2} \tag{3}$$

The idea is to consider cable 1 and cable 2 as one virtual cable whose velocity equals their average velocities. Equalling this average value with the velocity of drum 3, we ensure a parallelogram shape of the cables. Thus, ensuring the same length of the cables, constraint moments are exerted onto the MP to prevent the latter from rotating.

From the kinematic point of view, drum 1 has the same rotational velocity as motor B, i.e. $\omega_B = \omega_1$, drum 3 has the same velocity as motor A , i.e. $\omega_A = \omega_3$. Meanwhile, the velocity ω_2, results from the well-known differential formula:

$$\omega_{Carrier} = \frac{\omega_{Sun1} + \omega_{Sun2}}{2} \tag{4}$$

Here, the carrier velocity is ω_A while ω_B and ω_2 are the velocities of the two suns gears, respectively. Substituting in Eq. (4), leads to:

$$\omega_A = \frac{\omega_B + \omega_2}{2} \tag{5}$$

Therefore, the angular velocity ω_2 of drum 2 takes the form:

$$\omega_2 = 2\omega_A - \omega_B \tag{6}$$

As a consequence, the drum velocities can be expressed as a function of the motor velocities as follows:

$$\begin{bmatrix} \omega_1 \\ \omega_2 \\ \omega_3 \end{bmatrix} = \mathbf{J}_{DD} \begin{bmatrix} \omega_A \\ \omega_B \end{bmatrix}; \tag{7}$$

with $\mathbf{J}_{DD}$ being the kinematic Jacobian matrix of the transmission system expressed as:

$$\mathbf{J}_{DD} = \begin{bmatrix} 0 & 1 \\ 2 & -1 \\ 1 & 0 \end{bmatrix} \tag{8}$$

The cable speed $\dot{l}_i$ of the i-th cable is related to the corresponding winch angular velocity ω_i through the equation $\dot{l}_i = r_w\omega_i$, r_w being the radius of the drum. Upon combining this relation with Eq. (7), one obtains a mapping between motor speeds and cable uncoiling speeds. To obtain a complete model, the other two motors must be taken into account. Defining ω_C and ω_D as the angular velocities of the others two motors and ω_4, ω_5, ω_6 and ω_7 as the angular velocities of the drums connected to those two motors, the related cables create two parallelogram architectures and the following relationships are satisfied:

$$\omega_C = \omega_4 = \omega_5 \tag{9}$$

$$\omega_D = \omega_6 = \omega_7 \tag{10}$$

As a result, the drum velocities are expressed as a function of the motor velocities as follows:

$$\begin{bmatrix}\omega_1\\ \omega_2\\ \omega_3\\ \omega_4\\ \omega_5\\ \omega_6\\ \omega_7\end{bmatrix} = \mathbf{J}^*_{DD}\begin{bmatrix}\omega_A\\ \omega_B\\ \omega_C\\ \omega_D\end{bmatrix} \tag{11}$$

with

$$\mathbf{J}^*_{DD} = \begin{bmatrix}1 & 0 & 0 & 0\\ 2 & -1 & 0 & 0\\ 0 & 1 & 0 & 0\\ 0 & 0 & 1 & 0\\ 0 & 0 & 1 & 0\\ 0 & 0 & 0 & 1\\ 0 & 0 & 0 & 1\end{bmatrix} \tag{12}$$

3.2 Cable-driven parallel robot

A_i and B_i are cable exit points and cable anchor points, respectively. The following vectors are used throughout the rest of the paper:

- ${}^0\mathbf{a}_i$: Cartesian coordinate vector of point A_i expressed in $\mathscr{F}_0$;
- ${}^0\mathbf{b}_i$: vector pointing from O_0 to B_i expressed in $\mathscr{F}_0$;
- ${}^0\mathbf{l}_i$: ith cable vector, pointing from A_i to B_i expressed in $\mathscr{F}_0$;
- ${}^0\mathbf{p}$: Cartesian coordinate vector of point P expressed in $\mathscr{F}_0$;

3.2.1 Instantaneous Kinematics In this analysis the cable-loop system is considered as a single cable, namely, cables $\mathscr{L}_1$ and $\mathscr{L}_2$ are considered as $\mathscr{L}_{12}$. Six is the total number of cables considered, thus, three are the parallelogram architectures.
In frame $\mathscr{F}_0$, the loop-closure equation of the CDPR is:

$${}^0\mathbf{l}_i = {}^0\mathbf{b}_i - {}^0\mathbf{a}_i \tag{13}$$

with $i = 1,\dots,6$. The vector ${}^0\mathbf{b}_i$ can be be easily expressed in the function of the rotation matrix ${}^0\mathbf{R}_1$ between $\mathscr{F}_0$ and $\mathscr{F}_1$, ${}^1\mathbf{b}_i$ (position vector of B_i in the mobile frame) and ${}^0\mathbf{p}$ (origin vector of the mobile frame). Leading to:

$$\overrightarrow{A_iB_i} = l_i\,{}^0\mathbf{u}_i = \overrightarrow{A_iO_0} + \overrightarrow{O_0P} + \overrightarrow{PB_i} = -{}^0\mathbf{a}_i + {}^0\mathbf{p} + {}^0\mathbf{R}_1\,{}^1\mathbf{b}_i \tag{14}$$

The rotation matrix ${}^0\mathbf{R}_1$ from $\mathscr{F}_0$ to $\mathscr{F}_1$ is the identity matrix as the MP does not rotate theoretically:

$${}^0\mathbf{R}_1 = \begin{bmatrix}1 & 0 & 0\\ 0 & 1 & 0\\ 0 & 0 & 1\end{bmatrix} \tag{15}$$

The cable lengths are computed knowing the MP pose.
Remain to be defined:

- ${}^0\mathbf{u}_i = \frac{{}^0\mathbf{l}_i}{{}^0l_i}$: the cable unit vector;
- $\boldsymbol{\tau}_i = -\tau_i\,{}^0\mathbf{u}_i$: the ith cable tension vector;
- τ_i: magnitude of the i-th cable tension;

Upon differentiation of Eq. (14) with respect to time, we obtain:

$$\dot{l}_i\,{}^0\mathbf{u}_i + l_i\frac{d^0\mathbf{u}_i}{dt} = {}^0\dot{\mathbf{p}} + \frac{d^0\mathbf{b}_i}{dt} - \frac{d^0\mathbf{a}_i}{dt} \tag{16}$$

$\mathbf{a}_i$ being constant in $\mathscr{F}_0$, $\frac{d^0\mathbf{a}_i}{dt} = 0$. Replacing the time derivative of ${}^0\mathbf{u}_i$ and ${}^0\mathbf{b}_i$ by the cross product of the vector angular velocity, respectively $\dot{\boldsymbol{\beta}}_i$ and $\dot{\boldsymbol{\psi}}$ and the vector itself, leads to:

$$\dot{l}_i\,{}^0\mathbf{u}_i + l_i(\dot{\boldsymbol{\beta}}_i \times {}^0\mathbf{u}_i) = {}^0\dot{\mathbf{p}} + (\boldsymbol{\omega}_p \times {}^0\mathbf{b}_i) \tag{17}$$

Where $\dot{\boldsymbol{\beta}}_i$ is the angular velocity of the ith cable expressed in $\mathscr{F}_0$ and $\boldsymbol{\omega}_p$ is the angular velocity of the MP. To eliminate the passive variables, Eq. (17) is multiplied by ${}^0\mathbf{u}_i{}^T$,

$$\dot{l}_i\,{}^0\mathbf{u}_i^T\,{}^0\mathbf{u}_i + l_i\,{}^0\mathbf{u}_i^T(\dot{\boldsymbol{\beta}}_i \times {}^0\mathbf{u}_i) = {}^0\mathbf{u}_i^T\,{}^0\dot{\mathbf{p}} + {}^0\mathbf{u}_i^T(\boldsymbol{\omega}_p \times {}^0\mathbf{b}_i) \tag{18}$$

considering that:

1. The first term contains the dot product of the unit vector by it-self that leads to the norm of the unit vector, which is one.
2. The second term contains the dot product between ${}^0\mathbf{u}_i^T$ and $(\dot{\boldsymbol{\beta}}_i \times {}^0\mathbf{u}_i)$. Being the two latter vectors ortoghonal for the properties of the cross product, this term is null.

As a consequence, Eq. (18) takes the form:

$$\dot{l}_i = {}^0\mathbf{u}_i^T\,{}^0\dot{\mathbf{p}} + \boldsymbol{\omega}_p^T({}^0\mathbf{b}_i \times {}^0\mathbf{u}_i) \tag{19}$$

From Eq. (19), the relationship between the MP twist $\mathbf{t} = [\dot{\mathbf{p}}, \boldsymbol{\omega}_p]^T$ and the cable velocity vector $\dot{\mathbf{l}}$ can be expressed in a matrix form as:

$$\mathbf{A}\mathbf{t} = \mathbf{B}\dot{\mathbf{l}} \tag{20}$$

A and **B** being the forward Jacobian matrix and the inverse Jacobian matrix of the CDPR expressed as:

$$\mathbf{A} = \begin{bmatrix} {}^0\mathbf{u}_{12}^T & ({}^0\mathbf{b}_{12} \times {}^0\mathbf{u}_{12}) \\ {}^0\mathbf{u}_3^T & ({}^0\mathbf{b}_3 \times {}^0\mathbf{u}_3) \\ {}^0\mathbf{u}_4^T & ({}^0\mathbf{b}_4 \times {}^0\mathbf{u}_4) \\ {}^0\mathbf{u}_5^T & ({}^0\mathbf{b}_5 \times {}^0\mathbf{u}_5) \\ {}^0\mathbf{u}_6^T & ({}^0\mathbf{b}_6 \times {}^0\mathbf{u}_6) \\ {}^0\mathbf{u}_7^T & ({}^0\mathbf{b}_7 \times {}^0\mathbf{u}_7) \end{bmatrix}, \mathbf{B} = \mathbf{I}_6 \tag{21}$$

The angular velocity ω_p of the embedded pulley is a function of its radius r_p and the difference between cable 2 and cable 3 velocities:

$$\omega_p = \frac{\dot{l}_2 - \dot{l}_1}{2r_p} \tag{22}$$

By adding this equation to the previous ones, we obtain the global Jacobian matrices :

$$\mathbf{A}_g \, \mathbf{t}_g = \mathbf{B}_g \, \dot{\mathbf{l}}_g \tag{23}$$

$$\mathbf{A}_g = \begin{bmatrix} {}^0\mathbf{u}_{12}^T & ({}^0\mathbf{b}_{12} \times {}^0\mathbf{u}_{12}) & 0 \\ {}^0\mathbf{u}_3^T & ({}^0\mathbf{b}_3 \times {}^0\mathbf{u}_3) & 0 \\ {}^0\mathbf{u}_4^T & ({}^0\mathbf{b}_4 \times {}^0\mathbf{u}_4) & 0 \\ {}^0\mathbf{u}_5^T & ({}^0\mathbf{b}_5 \times {}^0\mathbf{u}_5) & 0 \\ {}^0\mathbf{u}_6^T & ({}^0\mathbf{b}_6 \times {}^0\mathbf{u}_6) & 0 \\ {}^0\mathbf{u}_7^T & ({}^0\mathbf{b}_7 \times {}^0\mathbf{u}_7) & 0 \\ \mathbf{0}_3^T & \mathbf{0}_3^T & 1 \end{bmatrix}, \mathbf{t}_g = \begin{bmatrix} \dot{\mathbf{p}} \\ \boldsymbol{\omega_p} \\ \dot{\alpha} \end{bmatrix} \tag{24}$$

$$\mathbf{B}_g = \begin{bmatrix} \frac{1}{2} & \frac{1}{2} & 0\,0\,0\,0\,0 \\ 0 & 0 & 1\,0\,0\,0\,0 \\ 0 & 0 & 0\,1\,0\,0\,0 \\ 0 & 0 & 0\,0\,1\,0\,0 \\ 0 & 0 & 0\,0\,0\,1\,0 \\ 0 & 0 & 0\,0\,0\,0\,1 \\ -\frac{1}{2r_p} & \frac{1}{2r_p} & 0\,0\,0\,0\,0 \end{bmatrix}, \dot{\mathbf{l}}_g = \begin{bmatrix} \dot{l}_1 \\ \dot{l}_2 \\ \dot{l}_3 \\ \dot{l}_4 \\ \dot{l}_5 \\ \dot{l}_6 \\ \dot{l}_7 \end{bmatrix} \tag{25}$$

Thus, the cable uncoiling speeds from a prescribed twist of the end-effector can be found solving the Eq. (23) as $\dot{\mathbf{l}} = \mathbf{J}_m \mathbf{t}$, where $\mathbf{J}_m = \mathbf{B}_g^{-1} \mathbf{A}_g$.

3.2.2 Static equilibrium The static equlibrium of the MP is obtained by analyzing its free-body diagram:

$$-\sum_{i=1}^{7} t_i \, {}^0\mathbf{u}_i + m \, {}^0\mathbf{g} \tag{26}$$

m is the MP mass and ${}^0\mathbf{g}$ is the gravity acceleration vector. The sum depends on the branches under tension, which are seven. Now we can express the equilibrium of the moments applied on the platform in the fixed frame respect to P:

$$-\sum_{i=1}^{7} t_i ({}^0\mathbf{R}_1 \, {}^1\mathbf{b}_i \times {}^0\mathbf{u}_i) + m({}^0\mathbf{c} - {}^0\mathbf{p}) \times {}^0\mathbf{g} = 0 \tag{27}$$

where ${}^0\mathbf{c}$ stands for the Cartesian position vector of the platform center of mass, which depends on the platform shape and architecture. For example, assuming ${}^0\mathbf{c} = {}^0\mathbf{p}$, simplifies the latter equation. Then, ${}^0\mathbf{d}_i = {}^0\mathbf{R}_1 \, {}^1\mathbf{b}_i \times {}^0\mathbf{u}_i$ is defined to have a more compact expression.
Since the studied platform is characterized by a cable-loop principle, we have also to consider the moment, defined as γ_p, introduced by the difference of the tensions between the two branches of the cable-loop (cable 1 and 2):

$$\gamma_p = r_p(\tau_1 - \tau_2) \tag{28}$$

From Eqs. (26) to (28), the static equilibrium of the MP and the embedded pulley is defined by the following equation:

$$\mathbf{W}\boldsymbol{\tau} + \mathbf{w}_e = \mathbf{0}_7 \tag{29}$$

where $\mathbf{W}$ is the wrench matrix, $\boldsymbol{\tau}$ is the cable tension vector and $\mathbf{w}_e$ is the external wrench.

$$\mathbf{W} = -\begin{bmatrix} {}^0\mathbf{u}_1 & {}^0\mathbf{u}_2 & {}^0\mathbf{u}_3 & {}^0\mathbf{u}_4 & {}^0\mathbf{u}_5 & {}^0\mathbf{u}_6 & {}^0\mathbf{u}_7 \\ {}^0\mathbf{d}_1 & {}^0\mathbf{d}_2 & {}^0\mathbf{d}_3 & {}^0\mathbf{d}_4 & {}^0\mathbf{d}_5 & {}^0\mathbf{d}_6 & {}^0\mathbf{d}_7 \\ -r_w & r_w & 0 & 0 & 0 & 0 & 0 \end{bmatrix} \tag{30}$$

$$\boldsymbol{\tau} = \begin{bmatrix} \tau_1 & \tau_2 & \tau_3 & \tau_4 & \tau_5 & \tau_6 & \tau_7 \end{bmatrix}^T \tag{31}$$

$$\mathbf{w}_e = \begin{bmatrix} m{}^0\mathbf{g}^T & m({}^0\mathbf{R}_1 \, {}^1\mathbf{c} \times {}^0\mathbf{g})^T & \gamma_p \end{bmatrix}^T \tag{32}$$

Basically, the wrench matrix maps the cable tension (joint space) into the external force applied on the end-effector (operational space). The cable tension vector $\boldsymbol{\tau}$ can be obtained from the inverse of the square wrench matrix $\mathbf{W}$ as long as it is not rank-deficient, namely, $\det(\mathbf{W}) \neq 0$:

$$\boldsymbol{\tau} = \mathbf{W}^{-1} \mathbf{w}_e \tag{33}$$

4 WORKSPACE ANALYSIS

This section deals with the analysis of the CDPR workspace considering different cable arrangements. For every possible external force-moment system $\mathbf{w}_e$, the moving platform will be in an equilibrium if and only if, Eq. (29), can be satisfied by a set of feasible cable tensions $\boldsymbol{\tau}$. A "feasible pose" is defined as a state of "full" equilibrium between the moving platform and the embedded pulley. The set of all feasible poses is called the "wrench-feasible workspace $\mathscr{F}$" (WFW) and is formally expressed as follows:

$$\mathscr{F} = \{(\mathrm{p}, \alpha) \in \mathbb{R}^3 \times \mathbb{R} : \forall \mathbf{w}_e \in \mathscr{W}_e, \exists \tau \in \mathscr{T}, \mathbf{W}\tau + \mathbf{w}_e = \mathbf{0}_7\} \quad (34)$$

where $\mathscr{W}_e$ is the set of external wrenches that can be applied on the MP, including the moment exerted on the embedded pulley. The available cable tension set is defined by $\mathscr{T}$, which is a function of the available motor torques and the Jacobian matrix $\mathbf{J}_D$ defined in Eq. (12). For the purpose of workspace analysis, we have only considered pure translations of the moving platform and the rotation of the embedded pulley. The parallelogram cable-loops are supposed to fully constrain the rotational motions of the MP.

Fig. 6 shows the boundary of the WFW $\mathscr{F}$ of the CDPR with a MP weighing 8kg and a moment γ_p exerted on the embedded pulley within the bounds [0.5, 0.5] Nm. The goal is to investigate the workspace for two different cases *i.e.*, with and without involving the parallelograms $A_4B_4B_5A_5$ and $A_6B_6B_7A_7$ shown in Fig. 1. The WFW boundary for the first case study, which only used four cables and did not involve the aforementioned parallelograms, is depicted in Fig. 6a. The transmission system is connected by two cables, while the other two cables are the consequence of the two parallelograms. The parallelograms are represented in two distinct cable layouts in the second case study. *i.e.*, (i) both parallelograms connected on the top plane of the MP, (ii) both parallelograms are vertically connected on the MP, one on the top and the other on the bottom plane. The boundary of the WFW for the second case study are shown in Figs. 6b and 6c.

It can be noticed that employing the parallelogram architecture enlarged the workspace; however, the second case study presented in Fig. 6b has maximum workspace and thus the configuration will be employed for the experiments.

5 PROTOTYPING AND EXPERIMENTATION

This section presents the CDSMG prototype and the experiments realized at LS2N, Nantes, France. The tests aimed to validate that the three parallelogram architectures prevent the MP from rotating and the cable loop, actuated through a transmission system, does actuate the rotational motion of the end-effector about a vertical axis. The prototype is tested with tra-

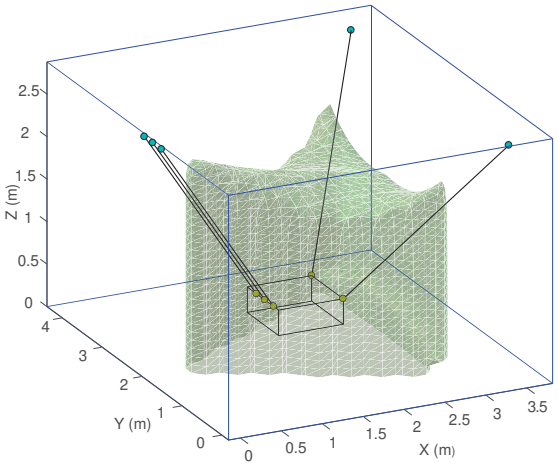

(a) Four cables configuration with a single parallelogram cable loop

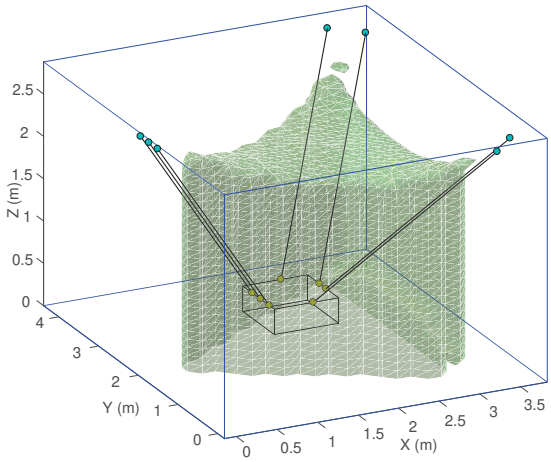

(b) Six cables configuration with three parallelograms and a cable loop (All three parallelograms connected on the top plane of the MP)

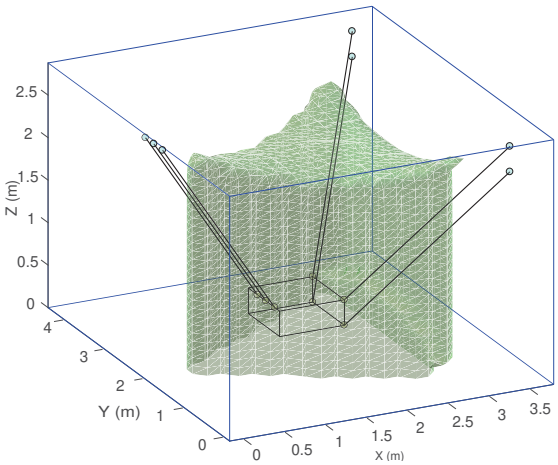

(c) Six cables configuration with three parallelograms and a cable loop (On the MP, one parallelogram is at the top, while the other two are connected vertically)

FIGURE 6: Wrench feasible workspace of the CDSMG for three cable arrangements with $m = 8$ kg and -0.5 Nm $\leq \gamma_p \leq 0.5$ Nm

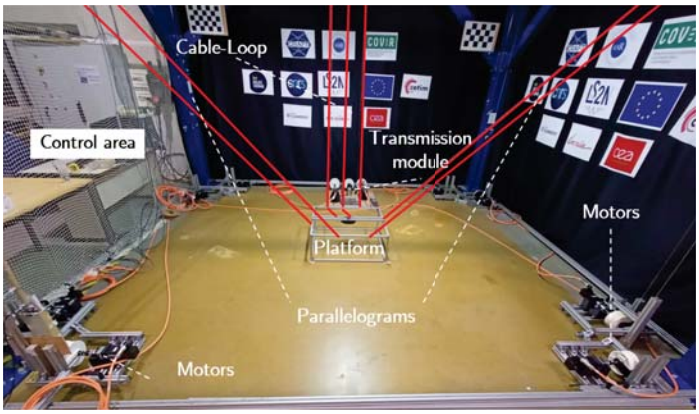

FIGURE 7: Prototype of the Cable-Driven Schönflies Motion Generator (CDSMG)

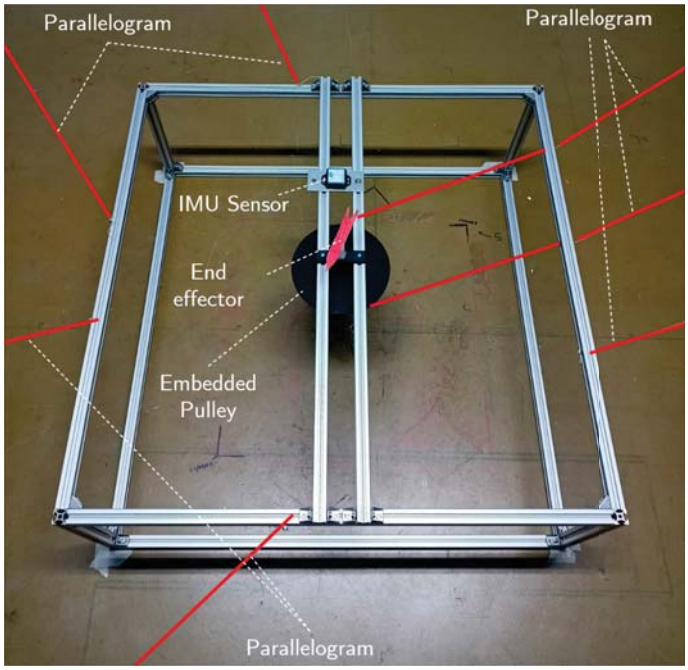

FIGURE 8: Moving-platform, embedded pulley and selected cable arrangement

jectories where translations and rotations of the end-effector are performed in sequence first and then combined.

5.1 Prototype presentation

The overall prototype architecture is shown in Fig. 7. A parallelepiped made of Bosch profiles with a pulley on the centre of the top rectangle is the platform adopted (Fig. 8). A red arrow, positioned on the pulley, is the end-effector of the CDSMG. The seven anchor points are fixed to the structure through knots in drilled holes. The position of the anchor points results from the fact that the bigger the parallelogram, larger the constraint moments exerted on the MP with the three parallelogram architectures. An Inertial Measurement Unit (IMU) was placed on the platform to correctly assess the oscillations during the experiments.

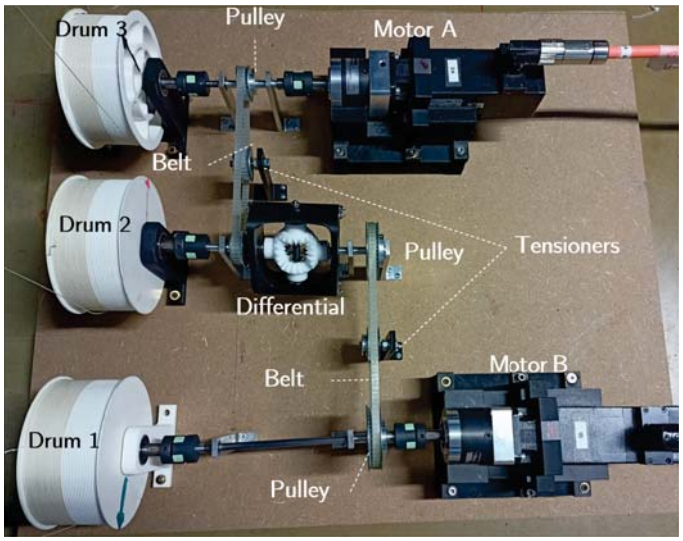

FIGURE 9: Transmission Prototype

The transmission module, shown in Fig. 9, was designed taking care of the following aspects:

1. ensure high stiffness of the components (differential and belts). In that way the position accuracy of the involved drums will benefit;
2. use of proper tensioners able to regulate the belt tension. This was done using solts instead of holes to adjust the component position at a later stage;
3. reduce the backlash in-between teeth of the conical gears of the differential, this was done by equipping the gears with adjustment systems (using nuts), to be able to adjust the distance between the gears during the assembly;
4. avoid using heavy materials for the components to reduce the inertia of the rotational parts, therefore, prefer light and noiseless polymeric materials; in that way, the dynamical performance will benefit;
5. comply with current standards regarding shaft, pulleys, gears and belts dimensioning.

The transmission system is grounded on the floor with counterweights since the forces acting on the drums are not negligible. Figure 10 shows the main hardware of the prototype, which consists of a PC (equipped with © MATLAB and © ControlDesk software), eight © PARKER SME60 motors and TPD-M drivers, a © dSPACE DS1007-based real-time controller and seven custom made winches. Each cable can exert a tension

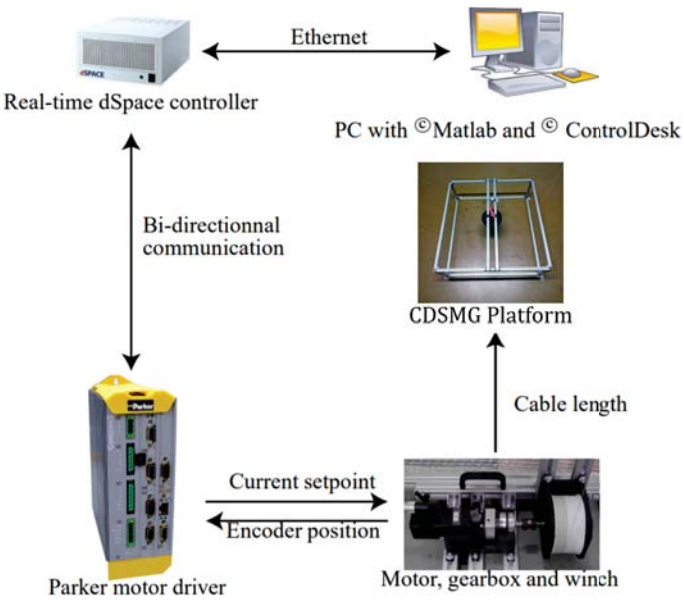

FIGURE 10: : Control architecture of the manipulator

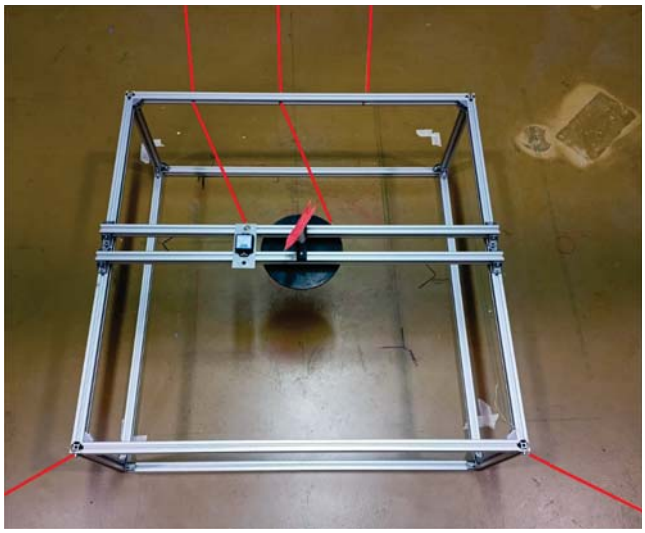

FIGURE 11: Platform without parallelograms, used as reference for the tests

up to 150 N to the MP. The maximum velocity of each cable is equal to 5.9 m/s. Pulleys are used to guide the cable from the drums to the platform's anchor points.

During the experiments, unlike the system described in Sec. 2, each of the four cables (4,5,6, and 7) forming the two parallelograms, was controlled by one motor each. This choice derives from the fact that the dimension of the 2-drums/1-shaft system (Fig. 1) was not compatible with the robot frame at hand. However, each pair of cables invloved in a parallelogram architecture was actuated using the same control scheme, thus making the use of the 2-drums/1-shaft system unnecessary.

5.2 Experiments

The experiments aim to test the effectiveness of the proposed parallelogram-arrangement architecture in preventing the parasitic tilts during the translational motions of the MP and the cable-loop circulation. Two primary experiments were carried out. The first, with the platform constrained by parallelograms to the frame as shown in Fig. 8. The second, where the number of cables was reduced to four, removing two parallelograms to the CDSMG as illustrated in Fig. 11.

In the first experiment, the prototype of the CDSMG is tested based on the trajectories described in 5.3. Every test was conducted while taking care that all cables were taut and that the platform was always in the same initial pose. An IMU was used to record the MP inclinations during the trajectories and cameras were used to record both the platform and the transmission system to be able to detect possible issues in a second phase.

The second experiment was conducted substituting a single cable to the two parallelogram architectures not involved in the cable-loop. With this test, we wanted to compare the CDSMG to the manipulator free of the two simple parallelogram architectures, proving the effectiveness of the proposed CDSMG.

5.3 Trajectories

The trajectory for evaluating the parallelogram's performance concerning the platform orientation is explained in this section. The trajectory is made up of several motion sequences. Five sequences of pure translational motions of the MP are performed first, followed by a pure rotation of the embedded pulley. Both of the aforementioned motions are combined in the trajectory's final sequence. Each sequence of the trajectory is defined using a fifth order polynomial. The following is a step-by-step description of each sequence:

1. pure translational motion along the positive z-axis of the MP from point P_0 to point P_1 ($0s \le t \le 10s$);
2. diagonal motion in the xy-plane along the positive x and y axes from point point P_1 to point P_2 ($10s \le t \le 20s$);
3. diagonal motion in the xy-plane from point P_2 to point P_1 ($20s \le t \le 30s$);
4. diagonal motion in the xy-plane along negative x and positive y axes from point P_1 to point P_3 ($30s \le t \le 40s$);
5. diagonal motion in xy-plane from point P_3 to point P_1 ($40s \le t \le 50s$);

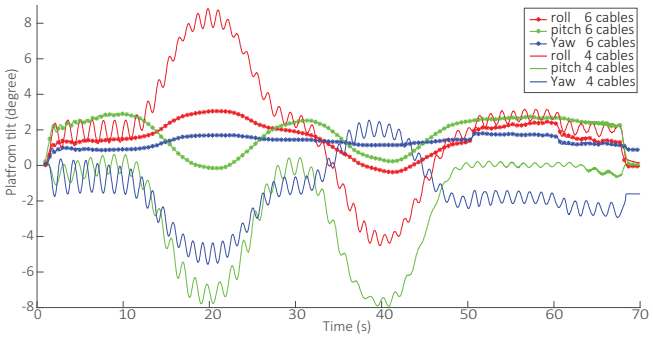

FIGURE 12: MP inclinations measured by an IMU sensor for the CDSMG with three parallelogram cable-loops (6 cables used) and the manipulator with one parallelogram cable-loop only (4 cables used)

6. pure anti-clockwise rotational motion of the embedded pulley at point P_1 ($50s \leq t \leq 60s$);
7. the last sequence of the trajectory consists of a translational motion of the MP from point P_2 to point P_1 combined with a clockwise rotation of the embedded pulley ($60s \leq t \leq 70s$).

6 Result Analysis

The experiments are showed in the Video[1]. During the tests, the MP inclinations were recorded via the IMU sensor. This allowed us to objectively monitor the magnitude of the tilts. From the video, it is easy to see that the parallelogram architecture makes a difference when compared to the robot exempt from these.

6.1 Analysis of the Results

In Fig. 12 the orientation angles measured with the IMU sensor are represented in a Cartesian coordinate system where the x-axis stands for the time and the y-axis stands for the roll, pitch and yaw angles. It can be noted that the dotted line, which describes the robot proposed in this paper, has far fewer peaks than the case without parallelograms (normal line). This underlines the high stability of the CDSGM robot. In the first experiment, the MP inclinations never exceeded 3°. While during the second experiment, not having the parallelograms, the MP inclination measured reached 10° degrees. In addition, as can be noticed in Fig. 12 and from the video, the tilts in the second case are highly frequent. Despite the small initial errors of orientation, the platform remained stable during the trajectories avoiding frequent oscillations as in the second experiment. In the first attempt, as a result of the parallelograms, the MP did not change its orientation when subjected to the pulley rotation. In the second case, the rotation of the pulley affected constantly the orientation of the robot.

6.2 Discussion

The results obtained are positive and in line with our expectations, the parallelogram architecture makes the difference if compared to the case free of it. The difference of maximum tilt observed in the two cases (3° vs 10°) is tangible proof that the proposed robot is effective. The continuous oscillations of the roll, pitch, yaw angles show the instability of the system with a lack of cables.

Referring to the case with six cables (Fig. 12), it can be seen that the yaw angle, the one about the z-axis, is small compared to the roll and the pitch angles of MP. The asymmetric arrangement of the cable around the platform favours the rotations around some degrees of rotation over others. The tilts around the x-axis and the y-axis have greater variations over time due to less contribution of the parallelograms. The reasons stand both cable arrangement, which is not optimal and in the robot modelling errors. The proposed CDSMG seems not to be affected by the external torque exerted by the cable loop, making it robust and reliable.

6.3 Issues encountered and solutions

During the experiments, weights were added to the platform to test the system in case of unexpected events. Tooth jumps of the belts occurred in the transmission system due to the higher amount of torque required by the motors. This problem was solved by tensioning the belts.

The test highlighted the fact that in the case of initial malpositioning of the platform the wrong orientation was maintained during the whole trajectory. To overcome this issue, we took care to reposition the platform in its original position, checking that all cables were seated in their respective pulley. The manufacturing errors in the transmission systems and the current disposition of the cable, which is not optimal and symmetric, may be identified as the causes of the remaining orientation errors. To resolve these issues, the cables should be positioned differently using, for example, an optimizing algorithm and the transmission should be designed with more care and detail.

7 Conclusions and Future Work

The motivation of this paper was to limit the unwanted rotations of the mobile platform of a Cable-Driven Schönflies-Motion Generator, CDSMG for brevity. The three parallelograms around the moving platform are extremely effective in reducing the parasitic inclinations of the MP. Constraining pairs of cables to have the same lengths and remain parallel,

[1] https://uncloud.univ-nantes.fr/index.php/s/Ker9YNgE5ry8MpF

successfully proves this architecture to be able to prevent parasitic tilts. In addition, the results are in agreement with the experiments carried out in [19] for a planar cable-driven parallel robot.

The objective was achieved thanks to a transmission module containing a differential mechanism. The latter permits to control the length of a parallelogram architecture and the circulation of the cable loop. The experiments showed that the solution proposed is effective and efficient. The MP inclinations never exceeded three degrees, which, for the authors, is considered a success. Meanwhile, the experiments conducted with only one parallelogram architecture revealed the usefulness of our design.

Although the experiments are promising, there is still plenty of work to be done in order to improve the positioning accuracy of the end-effector and reduce the MP oscillations. The transmission module should be assembled with method and accuracy. Additionally, the actual base of the transmission is made of wood, the use of a steel base will ensure the coaxiality of the shafts in the transmission system. Most of the components of the transmission and the MP are 3D printed, future work should deal with substituting those components with machining ones.

A further step is to carry out experiments using moving-platorms with different cable arrangements. To achieve the proper configuration the exit and the anchor point should be chosen following a proper design strategy, maximizing, for example, the workspace and the wrench capability of the CDSMG.

ACKNOWLEDGMENT

This work was supported by the ANR CRAFT project, grant ANR-18-CE10-0004, `https://anr.fr/Project-ANR-18-CE10-0004`, the Erasmus+ project and the RFI AtlanSTIC2020 CREATOR project. Assistance provided by Mr. Marceau Métillon through the experimentation process is highly appreciated.

REFERENCES

[1] Lambert, C., Nahon, M., and Chalmers, D., 2007. "Implementation of an aerostat positioning system with cable control". *IEEE/ASME Transactions on Mechatronics,* ***12***(1), pp. 32–40.

[2] Bostelman, R., Albus, J., Dagalakis, N., Jacoff, A., Gross, J., et al., 1994. "Applications of the nist robocrane". In Proceedings of the 5th International Symposium on Robotics and Manufacturing, Vol. 5.

[3] Gagliardini, L., Caro, S., Gouttefarde, M., and Girin, A., 2016. "Discrete reconfiguration planning for cable-driven parallel robots". *Mechanism and Machine Theory,* ***100***, pp. 313–337.

[4] Kawamura, S., Kino, H., and Won, C., 2000. "High-speed manipulation by using parallel wire-driven robots". *Robotica,* ***18***(1), pp. 13–21.

[5] Perreault, S., Cardou, P., Gosselin, C. M., and Otis, M. J.-D., 2010. "Geometric Determination of the Interference-Free Constant-Orientation Workspace of Parallel Cable-Driven Mechanisms". *Journal of Mechanisms and Robotics,* ***2***(3), 07. 031016.

[6] Nguyen, D. Q., Gouttefarde, M., Company, O., and Pierrot, F., 2014. "On the analysis of large-dimension reconfigurable suspended cable-driven parallel robots". In 2014 IEEE international conference on robotics and automation (ICRA), IEEE, pp. 5728–5735.

[7] Manubens, M., Devaurs, D., Ros, L., and Cortés, J., 2013. "Motion planning for 6-d manipulation with aerial towed-cable systems". In Robotics: Science and Systems (RSS), p. 8p.

[8] Platis, A., Rasheed, T., Cardou, P., and Caro, S., 2018. "Isotropic design of the spherical wrist of a cable-driven parallel robot". In *Advances in Robot Kinematics 2016*. Springer, pp. 321–330.

[9] Lessanibahri, S., Cardou, P., and Caro, S., 2020. "A cable-driven parallel robot with an embedded tilt-roll wrist". *Journal of Mechanisms and Robotics,* ***12***(2).

[10] Siciliano, B., 1999. "The tricept robot: Inverse kinematics, manipulability analysis and closed-loop direct kinematics algorithm". *Robotica,* ***17***(4), pp. 437–445.

[11] Mottola, G., Gosselin, C., and Carricato, M., 2019. "Dynamically feasible motions of a class of purely-translational cable-suspended parallel robots". *Mechanism and Machine Theory,* ***132***, pp. 193–206.

[12] Pott, A., Tempel, P., Verl, A., and Wulle, F., 2019. "Design, implementation and long-term running experiences of the cable-driven parallel robot caro printer". In International Conference on Cable-Driven Parallel Robots, Springer, pp. 379–390.

[13] Longval, J. M., and Gosselin, C., 2019. "Dynamic Trajectory Planning and Geometric Analysis of a Two-Degree-of-Freedom Translational Cable-Suspended Planar Parallel Robot Using a Parallelogram Cable Loop". *Journal of Mechanisms and Robotics,* ***11***(2), 02. 020903.

[14] Alikhani, A., Behzadipour, S., Ghahremani, F., Alasty, A., and Sadough Vanini, S. A., 2009. "Modeling, control and simulation of a new large scale cable-driven robot". In International design engineering technical conferences and computers and information in engineering conference, Vol. 49040, pp. 11–16.

[15] Mattioni, V., Ida, E., Carricato, M., et al., 2021. "Design of a planar cable-driven parallel robot for non-contact tasks". *Applied Sciences,* ***11***(20), p. 9491.

[16] Angeles, J., Caro, S., Khan, W., and Morozov, A., 2006. "Kinetostatic design of an innovative schönflies-motion generator". *Proceedings of the Institution of Mechanical Engineers, Part C: Journal of Mechanical Engineering Science,* ***220***(7), pp. 935–943.

[17] Pott, A., and Miermeister, P., 2018. "Workspace and interference analysis of cable-driven parallel robots with an unlimited rotation axis". In *Advances in Robot Kinematics 2016*. Springer, pp. 341–350.

[18] Fortin-Côté, A., Faure, C., Bouyer, L., McFadyen, B. J., Mercier, C., Bonenfant, M., Laurendeau, D., Cardou, P., and Gosselin, C., 2018. "On the design of a novel cable-driven parallel robot capable of large rotation about one axis". In *Cable-Driven Parallel Robots*. Springer, pp. 390–401.

[19] Etienne, L., Cardou, P., Métillon, M., and Caro, S., 2021. "Design of a planar cable-driven parallel crane without parasitic tilt". In International Design Engineering Technical Conferences and Computers and Information in Engineering Conference, Vol. 85444, American Society of Mechanical Engineers, p. V08AT08A038.

[20] Métillon, M., Cardou, P., Subrin, K., Charron, C., and Caro, S., 2021. "A cable-driven parallel robot with full-circle end-effector rotations". *Journal of Mechanisms and Robotics,* ***13***(3), p. 031017.